Vol. 75: 181–199, 2018
https://doi.org/10.3354/cr01518

CLIMATE RESEARCH
Clim Res

Published online August 9

Statistical modelling of snow cover dynamics in the Central Himalaya Region, Nepal

J. Weidinger[1,*], L. Gerlitz[2], B. Bechtel[1], J. Böhner[1]

[1]CEN - Center for Earth System Research and Sustainability, Institute of Geography, University of Hamburg, 20146 Hamburg, Germany

[2]GFZ - German Research Centre for Geosciences, Helmholtz Centre Potsdam, 14473 Potsdam, Germany

ABSTRACT: Snow cover modelling is primarily focussed on snow depletion in the context of hydrological research. Degree-day or temperature index models (TIMs) as well as energy balance models (EBMs) are conventional to quantify catchment runoff. Whereas the former exploit relationships between snow (and/or ice) melt and air temperatures, the latter rest upon quantifying melt as the deviation from heat balance equations. However, the 2 approaches contain distinct drawbacks. For example, increasing temporal resolution decreases the accuracy of TIMs, and no spatial variability is provided, whereas EBMs have large dataset requirements for climate, landscape and soil properties. Nevertheless, detailed knowledge about shifts in seasonal ablation times and spatial distribution of snow cover is crucial for understanding hydrological systems, plant distribution and various other research interests. Therefore, we propose a statistical model based on a combination of high resolution spatio-temporal climate datasets and climate-related topographic data, which were obtained by meteorological network stations, remote sensing and GIS analysis. The main objectives were to identify suitable inputs and to develop a robust binary snow distribution model that enables the mapping of major physical processes controlling snow accumulation, melt and stagnation in a high mountain environment in the Gaurishankar Conservation Area in Nepal. We used the random forest technique, which represents a state of the art machine learning algorithm. The snow distribution was predicted very accurately with high spatio-temporal resolution (daily on 0.5 × 0.5 km), with hit rates of around 90 % and an overall model accuracy of 90.8 % compared to independent Moderate Resolution Imaging Spectroradiometer (MODIS) observations.

KEY WORDS: Snow cover · Remote sensing · MODIS · Statistical modelling · Himalaya · Random forest

1. INTRODUCTION

The integration of robust snow cover or snow parameter models is a classic feature in hydrological runoff simulations or ecological habitat modelling (Hiemstra et al. 2006, Shrestha et al. 2012, Rohrer et al. 2013, Carlson et al. 2015) and thus requires reliable input data. Snow cover is not only one of the most dynamic properties of the cryosphere from an (intra)diurnal or seasonal point of view (Gao et al. 2006), but it is also expected to be one of the fastest-changing climate features under current climate warming (Stocker et al. 2013). The close relationship between the spatial distribution of snow cover and plant communities additionally leads to major impacts on mountain ecosystems and their biota (Litaor et al. 2008, Grabherr et al. 2010, Chen et al. 2011). According to Gao et al. (2012), snow cover extent stretches from 1 % in August up to 87 % in February with a mean of 35 ± 20 % (SD) for eastern Tibet, and the snow cover fraction over the whole Tibetan Plateau (elevation >2000 m a.s.l.) ranges from an average minimum of 5.3 % between March and August to a mean maximum of around 33 % in Febru-

*Corresponding author: johannes.weidinger@uni-hamburg.de

ary (Pu et al. 2007). In eastern Tibet, high interannual variations in snow cover occur (Immerzeel et al. 2009), with a negative correlation ($R = -0.651$, $p < 0.001$) between the duration of snow-free periods and elevation. Snow cover shows an increase at higher elevation, induced by enhanced orographic precipitation, whereas lower elevations show a decreasing trend in recent years, controlled through higher air temperatures (Gao et al. 2012).

Beside spatio-temporal characteristics, the physical properties of snow are highly relevant (Paudel & Andersen 2011). The density, thermal conductivity, permeability and optical properties of snow are both interdependant and also highly dependent on the overlying atmosphere and underlying ground (Domine et al. 2008). Alterations in snow density, for example due to snow temperature changes, result in dry or wet metamorphism throughout freeze–thaw cycles. Therefore, snow cover has a strong regulating function for latent heat fluxes (Rastner et al. 2009, Zaitchik & Rodell 2009, Endrizzi et al. 2014). According to Wiscombe & Warren (1980), the unique radiative properties of snow allow 3 different allocations: (1) In the visible spectrum, snow appears white for its high albedo but is affected by light-absorbing impurities. (2) Within the near-infrared spectrum, snow appears 'grey' and is mainly influenced by grain size. (3) In thermal infrared wavelengths, snow appears 'black' as it emits almost no thermal radiation. These characteristics are exploited in remote sensing techniques to gain strong delineations in relation to other surfaces (Domine et al. 2008). Furthermore, the low thermal conductivity, low roughness and unique spectral reflectance of snow influence the global energy balance, e.g. due to rapid changes in albedo after snow events or melting processes (Shrestha et al. 2012, Hernández-Henríquez et al. 2015). As a consequence of these changes in snow cover, feedback effects, such as stronger surface heating and higher water availability through snow melt (Stieglitz et al. 2001), can occur within the whole climate system and its sub-systems. Well known examples for snow-influenced circulation patterns are the monsoon circulation or local mountain–valley wind systems.

However, not only large- or macro-scale ($>10^3$ km) effects, such as a high degree of snow coverage over the Tibetan Plateau affect climate, but also, in particular, aspects from minor meso-γ-scale ($<10^1$ km) to micro-γ-scale ($<10^{-3}$ km), have significant effects on plant ecology, soil properties and topo-climate (Böhner & Antoni 2009, Vesterdal et al. 2013). At this scale, snow cover has an insulating function, supplies water, regulates permafrost, protects soil and shelters vegetation against late frost events (Domine et al. 2008, Grimm et al. 2013). In high mountain regions, these variations are particularly high due to the complex topography and the related variation in slope aspect, irradiation and related climatic processes (Pedersen & Egholm 2013). In addition, snow cover influences the microclimate, especially during dry periods, in winter and at higher altitudes. Snow cover diminishes the latent heat transfer and thus increases radiative cooling, resulting in local katabatic wind systems and cold air pooling (Gerlitz et al. 2016a). Although the processes leading to temporal and spatial variations in snow cover, such as snow melt (near surface temperatures >0°C) and variability in snow fall (precipitation at air temperatures <0°C) seem rather trivial, there are many aspects to consider. For example, snow formation occurs above, as well as below, 0°C in different fractions between solid and liquid state (Auer 1974) and may form a consistent layer of snow cover, provided the surface temperatures are low enough. In complex high mountain environments, high insolation rates, as well as strong topographic variations, have a strong impact on snow cover dynamics (Stieglitz et al. 2001, Böhner et al. 2015), and thus result in a strong spatio-temporal variability of snow cover.

During recent decades, the development of reliable precipitation, snow fall or snow coverage datasets at high spatial and temporal resolutions has been a major focus, since such data represent an important input for climate impact models. In particular, models to analyse and predict runoff or other hydrological parameters, e.g. in Central Asian mountain regions or Himalayan catchments, at a weekly or monthly temporal scale are needed in order to asses and forecast hydrological risk (Tekeli et al. 2005, Endrizzi et al. 2014, Immerzeel et al. 2014, Apel et al. 2018, Panday et al. 2014). Yet, the measurement of snow cover and related parameters, such as snow height or water equivalent, is still inherently complex and prone to errors (Trnka et al. 2010). Therefore, the estimates of snow coverage are often based on meteorological parameters, which are more accessible. Temperature index or degree-day models, which exploit the empirical relationship of melting rates and air temperatures, have been used for over a century to approximate snow (and ice) melt (Jeníček et al. 2012) and have been widely applied and refined over the decades (Clyde 1931, Hoinkes & Steinacker 1975, Braithwaite 1995, Hock 2003, He et al. 2014). They represent the most common approach to quantifying melt based on the following advantages: (1) broad availability, easy interpolation and forecasting tech-

niques of air temperature datasets; (2) computationally modest; and (3) generally good model performance. Nevertheless, this approach has shortcomings with increasing temporal resolution and spatial variability, and does not directly account for snow accumulation (Hock 2003). Energy balance models represent another important branch of snow cover models, which quantify snow melt as the difference in energy balance equations (Blöschl et al. 1991, Marks et al. 1999, Liston & Elder 2006, Shrestha et al. 2012). Many state of the art snow cover models contain several other sub-parameter models, such as soil, snow pack, meteorological or water-budget models, to describe the energy and mass-balance equations as accurately as possible (Liston & Elder 2006, Shrestha et al. 2015).

Considerable progress has been made in the development of complex modelling techniques such as (coupled) multi-layer energy balance models (Dawson & Wilby 2001, Rastner et al. 2009, Sirguey et al. 2009, Alford & Armstrong 2010, Shrestha et al. 2012, Bokhorst et al. 2016) fortified with *in situ* measurements. The data assimilation method is an effective technique to improve the results of spatio-temporal snow cover models (Kwon et al. 2016). With this method, remote sensing datasets, such as snow cover fraction (Rodell & Houser 2004, Zaitchik & Rodell 2009), brightness temperatures (Durand et al. 2009, Kwon et al. 2017) and terrestrial water storage (Forman et al. 2012, Houborg et al. 2012), are assimilated into land surface or snow dynamics models. Additionally, innovative and simple approaches have been developed to grasp snow cover dynamics (Stanzel et al. 2008, Trnka et al. 2010). Another applied method to describe and model snow cover is the use of freely available reanalysis products, such as ERA-Interim (Berrisford et al. 2009, Brun et al. 2013). However, reanalysis products poorly represent the local-scale variability of near surface climates in complex high mountain terrain, due to their coarse spatial resolution (Gerlitz et al. 2015). In particular, meteorological micro-β- to meso-γ-scale atmospheric boundary layer processes — such as topographically induced variations of orographic precipitation, nocturnal cold air drainage, solar insolation and surface heating — are not explicitly resolved by large-scale climate models or reanalysis products (Böhner & Antoni 2009, Gerlitz 2015).

Steady amendments in snow cover modelling in general (Loth & Graf 1988, Essery 1999, Martinec et al. 2008, Franz & Karsten 2013, Endrizzi et al. 2014) and especially on the Tibetan Plateau (Immerzeel et al. 2009, Rohrer et al. 2013, Shrestha et al. 2015) — mainly within physical top-down approaches and with coarse resolution (>1 km) — were achieved in the past decades. Nevertheless, little attention has been paid to establish reliable statistical snow cover models with high spatial and temporal resolution in complex mountain terrains (Shrestha et al. 2015). Geostatistical approaches have been implemented in the field of topo-climatology and vegetation distribution modelling. However, spatially distributed statistical models have thus far not been applied for snow cover related problems. Given that physical models are often prone to biases, particularly in complex environments, a statistical model setup is a promising alternative. Statistical models stand out due to their ability to find important relationships in observed data, and thus allow us to identify, quantify and predict the dynamics of a target variable based on important predictors. Particularly in comparison with physically based models, they are characterized by a reduced demand for computational capacity and input data.

This study presents and evaluates a geo-statistical model for snow cover extent and recession in the Central Himalaya Region (Rolwaling Himal), based on a machine learning algorithm. Our goal was to accurately model the main physical processes of (1) snow accumulation and (2) snow recession resulting from snow melt and sublimation. A random forest algorithm was trained at a daily temporal and moderate spatial resolution (ca. 500 m) based on meteorological *in situ* measurements, remote sensing data (Moderate Resolution Imaging Spectroradiometer [MODIS] and Shuttle Radar Topography Mission [SRTM] products) and topographic parameters. The model was calibrated with processed data covering the period from 2013 until 2015 and tested against independent verification data in 2016. Therefore, in order to demonstrate the model's capacity to accurately predict the snow-covered area (SCA) on a daily scale, the modelled SCA from January to June 2016 was crosschecked with MODIS observations.

2. DATA BASE AND METHODICAL BACKGROUND

2.1. Study area

The research domain, shown in Fig. 1a, in the Central Himalaya Region (Rolwaling Himal) is located between Nepal and the northern adjacent autonomous region of Tibet (27.713 to 28.079° N and 86.097 to 86.688° E). This area covers approximately 2400 km^2

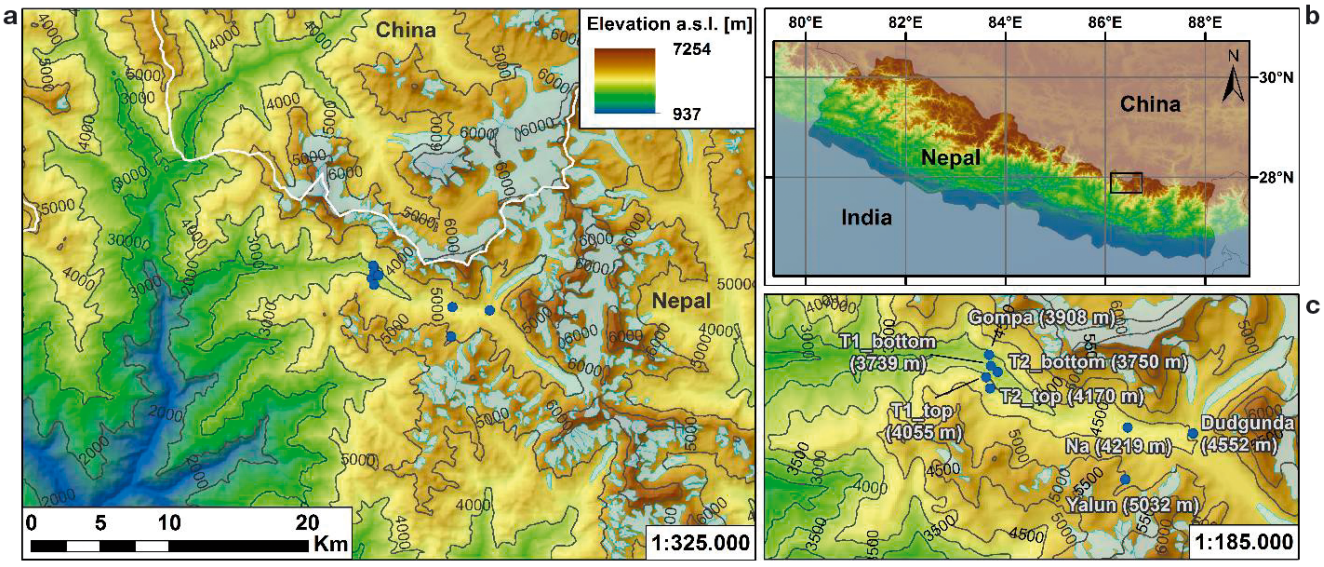

Fig. 1. (a) Modelling domain, (b) location of research area and (c) detailed positions of meteorological stations in the Rolwaling Himal. Glaciated areas (light blue) from Randolph Glacier Inventory, Version 6.0 (RGIC 2017)

of highly fissured mountain landscape and is partly situated in the Gaurishankar Conservation Area (Schickhoff et al. 2015). It covers steep terrain from ca. 1000 m up to 7250 m at the flanks of Cho Oyu (8188 m a.s.l.). The main valley in the research domain (Fig. 1a) is the Tama Koshi valley. Due to its windward position along the southern slopes of the Himalayan Arc and the direct impact of South Asian Monsoon circulation, the area receives high precipitation from mid-June until mid-September (Schwab et al. 2015; Table 1). Precipitation is subject to strong interannual variability, and occurs in solid form at higher altitudes, particularly during winter (Putkonen 2004, Anders et al. 2006, Shrestha et al. 2012). In general, the climate is characterized by warm and moist summers, due to advection of warm air from the Indian lowlands. During the cold and dry winters (December–February), occasional precipitation events are related to the passage of extra-tropical cyclones which follow the southern branch of the frontal Jetstream at the 200 hPa level. Particularly at higher elevations, winter precipitation falls predominantly as snow (Böhner 2006). The pre-monsoon season (March–May) is dominated by hot and dry weather with occasional rain events, whereas the post-monsoon season (October–November) is characterized by dry conditions (Shrestha et al. 2012). Besides large scale atmospheric controls and their seasonal variations, the climate of the target domain is strongly influenced by topo-climatic processes, which result in a strong spatial variability of temperature and precipitation at the micro-scale (Böhner 2006). The local wind systems within the valleys are particularly controlled by incoming solar shortwave radiation and thermal forcing, resulting in mountain–valley wind systems with characteristic nocturnal and diurnal air currents (Böhner et al. 2015). Table 1 provides basic climatic parameters for the described climatic patterns.

Table 1. Seasonal climatic averages measured at T1_bottom station at 3739 m a.s.l. Except for precipitation sums ($Prec_{sum}$), all other observations (air temperature [T], relative humidity [RH] and incoming solar radiation [Rad]) were averaged on a daily basis. Rad was only aggregated over daytime

Season	T_{min} (°C)		T_{mean} (°C)		T_{max} (°C)		RH (%)		Rad (W m^{-2})		$Prec_{sum}$ (mm)	
	Mean	SD	Mean	SD	Mean	SD	Mean	SD	Mean	SD	Mean	SD
Winter	−6.4	3.0	−1.9	2.9	4.6	3.8	53.3	19.4	303.4	76.2	0.3	1.2
Pre-monsoon	−1.1	3.3	3.2	3.0	8.6	3.0	79.2	15.0	408.1	123.2	2.2	3.9
Monsoon	6.6	1.6	9.1	1.0	12.9	1.6	98.0	3.0	296.7	112.1	7.7	7.0
Post-monsoon	−1.3	2.6	2.7	2.3	8.2	2.6	71.5	23.5	328.1	71.4	1.1	4.9

2.2. *In situ* measurements

As our aim was to develop a statistical model which is able to explain the snow cover dynamics in a high mountain area, suitable meteorological inputs are crucial, especially for spatial analysis (Soria-Auza et al. 2010, Immerzeel et al. 2014). Therefore, a recently installed meteorological network was used to obtain data of near surface air temperatures, global irradiance and precipitation at high temporal resolution. All 7 automatic weather stations are deployed in the Rolwaling valley (Fig. 1c). Global irradiance is monitored using an Onset™ HOBO™ S-LIB-M003 pyranometer, calibrated between 0 and 1280 W m^{-2} (accuracy ±10 W m^{-2}) and a spectral range from 300 to 1100 nm. Near-surface air temperatures are measured via the S-THB-M002, with a combined temperature and relative humidity sensor (accuracies ±0.21°C and ±2.5%) from the same supplier. Since no direct snow detection sensors were available, we used Onset™ HOBO™ S-RGB-M002 tipping-bucket rain gauges with an effective range of 0 to 127 mm h^{-1} and an accuracy of ±1.0% up to 20 mm h^{-1} (Synotech, www.synotech.de/produkte/datenblatt). For volumetric precipitation records, all tipping events inside the rain gauge were counted and summarised. The gauges were sheltered from wind with a protection ring surrounding the top opening. Since the network uses non-heated tipping sensors, snowfall events might not be traced correctly. Raised temperatures due to solar radiation during the day leads to melting of frozen precipitation in the buckets, and thus to delayed observations, which are removed from the dataset. All parameters except fluid deposition are measured at 3 min intervals and logged as a single mean after 15 min. The meteorological network was set up in April 2013 (first 5 stations) and was extended in October 2013 (last 2 stations), and has been continuously operating since then. Even though all sensors are suitable for high mountain regions, the rough environment of the Rolwaling Himal and some acts of vandalism led to several sensor failures and 2 station losses, which could only be replaced in the subsequent field campaign and thus caused several data gaps.

2.3. Remote sensing observations

For continuous daily spatio-temporal climatic data, MODIS/Terra Snow Cover Daily grids (L3 Global 500 m, Version 5), MODIS/Terra Land Surface Temperatures and Emissivity Daily grids (L3 Global 1 km, Version 5) and TRMM daily precipitation composites (Version 7: 0.25°, equivalent to 27.8 km spatial resolution) were resampled to the target resolution of the snow cover product via nearest neighbour regionalisation (Riggs et al. 2006, Wan 2006, Huffman et al. 2007). The automated snow-mapping MODIS/Terra snow cover algorithm is based on the satellite reflectances in bands 4 (0.545–0.565 µm) and 6 (1.628–1.652 µm) to calculate the normalised difference snow index (NDSI) according to Hall et al. (1995):

$$\mathrm{NDSI} = \frac{\text{band 4} - \text{band 6}}{\text{band 4} + \text{band 6}} \quad (1)$$

Additionally, automatic cloud detection, atmospheric correction and several pre-processings for different land cover types are included (Hall et al. 2002).

Land surface temperatures are generated from measurements in the thermal infrared bands 31 (10.78 to 11.28 µm) and 32 (11.77 to 12.27 µm) using the day–night split-window algorithm (Wan & Dozier 1996). For all MODIS datasets, the TERRA platform products were used without additional AQUA data due to better coverage of the research domain. Between 2013 and 2016, AQUA had approximately 20% fewer observations than TERRA, which is slightly higher than Wang et al. (2015) found for the whole Tibetan Plateau.

The TRMM-3B42RT daily composites are derived from passive microwave observations, which generally perform well for convective systems, but underestimate orographic rainfall induced by warm clouds over mountainous regions in advective regimes (Dinku et al. 2010). Since precipitation data with daily temporal resolution are needed for the model calibration, the TRMM product was implemented and interpolated to the spatial resolution of the MODIS snow cover product, despite the mentioned shortcomings (Huffman et al. 2007, Dinku et al. 2010).

In order to estimate the spatial distribution of topoclimatic parameters, an SRTM-derived digital elevation model (DEM) (Jarvis et al. 2008) was resampled and projected towards the modelling domain (500 m horizontal resolution). Table 2 provides information on all input variables based on remote sensing products. Inputs based on lower spatial resolution than the MODIS snow cover product were interpolated using a nearest neighbour approach, while inputs based on the DEM were aggregated deploying a cubic spline approach (Conrad et al. 2015)

2.4. Random forest based modelling approach

Random forest is a machine learning method defined as an ensemble of tree predictors, where each

Table 2. Overview of remote sensing products used in this study and their combinations with *in situ* measurements

Input parameter	Product and platforms	Original spatial resolution (km)	Temporal resolution (h)	Remarks
Surface temperature	MOD11A1, Ver. 5, MODIS	1.0 × 1.0[b]	24[c]	Dynamic
Warming rate[a]	MOD11A1, Ver. 5, MODIS	1.0 × 1.0[b]	24[c]	Dynamic
Precipitation	TRMM 3B42 RT, Ver. 7, GPM	27.8 × 27.8[b]	24[c]	Dynamic
Digital elevation model	SRTM, Ver. 4.1, CGIAR-CSI	0.09 × 0.09[b]	–	Static
Aspect[a]	SRTM, Ver. 4.1, CGIAR-CSI	0.09 × 0.09[b]	–	Static
Convergence index[a]	SRTM, Ver. 4.1, CGIAR-CSI	0.09 × 0.09[b]	–	Static
Solar insolation[a]	SRTM, Ver. 4.1, CGIAR-CSI	0.09 × 0.09[b]	24[c]	Static
Snow cover	MOD10A1, Ver. 5, MODIS	0.5 × 0.5	24	Dynamic

[a]Derived from former main input; [b]Resampled to MODIS snow cover product; [c]Available in higher temp. resolution

tree is built based on the values of an independently sampled vector (Breiman 2001). Random forests are generally based on classification and regression trees (CARTs), which can be either numerical (regression trees) or categorical (classification trees), and enable the identification of statistical patterns within data. By maximizing the homogeneity of a predictor variable at binary splits, datasets are gradually classified (Breiman et al. 1984). CARTs offer many advantages: (1) they are nonparametric; (2) they can be built without the need for preliminary variable selection; (3) their results are constant to monotone transformations of their predictor variables; and (4) they are not sensitive to outliers. However, they tend to strongly overfit the data without adjusted pruning (Timofeev 2004).

In random forests, two additional layers of randomness are added, by means of merging and bagging, i.e. a selection of random subsets of split variables at each node. Therefore, they perform very well in comparison to other state-of-the-art classifiers, such as discriminant analysis, support vector machines or artificial neural networks (Liaw & Wiener 2002, Yu et al. 2011). Random forests are employed in various research fields, such as speech recognition, species distribution modelling and remote sensing, as well as for predictions of future climate scenarios (Yu et al. 2011, Bechtel & Daneke 2012, Louppe et al. 2013, Belgiu & Drăguţ 2016, Gerlitz et al. 2016). Allocated in the emerging field of machine learning algorithms, this non-parametric technique is an ensemble approach, since a large number of 'weaker' learners is combined to form a stronger one. Random forests are particularly used for data mining approaches, since they are able to inductively generate a set of rules to explain relationships and dependencies within the inputs (Breiman 2001). In contrast to CART, trees in random forests can no longer be examined separately. Therefore, it seems that random forests tend to be 'black box' approaches, similar to artificial neural networks. However, to evaluate the performance of random forests, and for quality assessment, several metrics have been implemented. These allow random forests to be declared as 'grey boxes', since relative variable importance and other predictor estimates offer an insight into internal devolutions (Breiman 2001, 2002, Prasad et al. 2006).

Through the initial bagging, a form of bootstrap aggregation with replacement and left-out samples (out-of-bag; OOB), of the training data at the beginning of each single tree, an internal error rate verification is added. By testing each final tree with the OOB samples, it works as a surplus validation criterion to the proposed modelling approach:

$$Q(\boldsymbol{x}, j) = \sum_{k} I\left[h(\boldsymbol{x}, \boldsymbol{\Theta_k}) = j; (\boldsymbol{y}, \boldsymbol{x}) \notin T_{k,B}\right] / \sum_{k} I\left[(\boldsymbol{y}, \boldsymbol{x}) \notin T_{k,B}\right] \quad (2)$$

where $Q(\boldsymbol{x},j)$ is the OOB estimate of error rate, k is the number of trees, I is an indicator function, h is a classifier for $(\boldsymbol{x},\boldsymbol{\Theta_k})$, where $\boldsymbol{x}$ is an input vector and $\boldsymbol{\Theta_k}$ is a random vector $(\boldsymbol{y},\boldsymbol{x})$, j is the class resulting from h, and $T_{k,B}$ is the bagged (bootstrap) training dataset (Breiman 2001).

To evaluate the relative importance of each variable, 4 measures are implemented for classification. In the presented case, these performance measures allow us to evaluate the representation of the major physical processes in snow accumulation and snow recession. The 2 most essential random forest importance measures are mean decrease in accuracy (MDA) and mean decrease in node impurity (MDI), also known as mean decrease Gini coefficient (Liaw & Wiener 2002). The MDA is defined as the average lowering of the margin across all cases (in-bags),

compared to randomly permuted values in the OOB. The margin is specified as the proportion of votes for its actual class subtracted by the maximum of the proportion of votes for each 'false' class. In contrast, the MDI as a Gini-criterion is the sum of decreases of the m^{th} variable (X_m) in node impurity $p(t)\Delta i(s_t,t)$ at all nodes (t), normalised by the number of trees (N_T) (Breiman 2002, Louppe et al. 2013):

$$Imp(X_m) = \frac{1}{N_T}\sum_{T}\sum_{t\in T:x(s_t)=X_m} p(t)\Delta i(s_t,t) \quad (3)$$

where $Imp(X_m)$ is the MDI, $p(t)$ is the proportion of N_T/N of all samples reaching t, $x(s_t)$ is the variable used in split (s_t) and Δi is the impurity measure (in this case the Gini index). According to Louppe et al. (2013), there are still several shortcomings in fully understanding variable importance measures. While Ishwaran (2007) gave a theoretical insight for the MDA, Strobl et al. (2007, 2008) found evidence that both variable importance functions are biased towards correlated variables. However, this was not confirmed in later experimental studies (Genuer et al. 2010). For the evaluation of the random forest performance, hit rates and overall accuracy are defined. While the hit rates simply are correctly predicted values normalised over positive and false predictions, the overall model accuracy is defined as:

$$A_j = \sum_j x_{t,j} p_j \,/\, \sum_j p_j \quad (4)$$

where A_j is the overall weighted model accuracy for all classes, $x_{t,j}$ are true positive predicted class records, and p_j are all predicted values. Further, in order to evaluate the performance of the developed SDM, an unweighted Kappa coefficient is used. It allows us to measure the agreement for the categorical items 'snow cover' vs. 'snow free' between the model's predictions and observations. Hereby, the Kappa coefficient permits the statistical consideration of the accordance by chance (Cohen 1960). The unweighted Kappa coefficient k is the remaining proportion of agreement, after the agreement by chance is removed:

$$k = \frac{p_o - p_e}{1 - p_e} \quad (5)$$

Here p_o is the proportion of units with agreement, p_e is the hypothetical proportion of expected agreement by chance, and $k = 1$ is a complete agreement between all categories. Breiman (2001) summarised the advantages of random forest as follows: (1) it does not overfit data; (2) it is relatively robust to outliers and noise; (3) it is faster than bagging or boosting; (4) it gives useful internal estimates of error, strength, correlation and variable importance; (5) it is simple and easily parallelised. Therefore, random forests are considered to be one of the most accurate general-purpose learning techniques available (Biau 2012).

To evaluate the effect of different input parameters within the random forest approach, a sensitivity analysis is conducted. For this purpose, mean values for each cell and parameter are calculated (and the statistical mode for the binary SNOWFALL parameter). These cell means serve as reference inputs and are used for one reference snow cover prediction of the final model. Afterwards, every cell of each input parameter is altered in the magnitude of the overall standard deviation σ (−σ and +σ) of that parameter within the whole modelling domain, to visualize its effect on the random forest approach.

3. MODEL DEVELOPMENT AND INPUT PARAMETER IMPLEMENTATION

3.1. Training setup of random forest

The introduced physical principles driving snow cover distributions and their seasonal characters result in a large spatio-temporal variability of snow cover in a complex high mountain environment. Aiming at a statistical representation of those processes, a statistical analysis of spatial snow cover dynamics was conducted using a random forest approach (R Core Team 2014, R Studio Team 2015). An inductive bottom-up strategy was applied to analyse spatio-temporal dependencies in raster data and deviated parameters. All grids were resampled to UTM zone 45 north within WGS84. To account for the physical processes described in Section 1, the predictor variables, as shown in Fig. 2, were selected within the model set up. They are discussed in detail in the following sections. Snow cover changes were selected through comparison with the identical cell of the following day. Only cells with observations for both days were included, and cells which did not change throughout the modelling period (e.g. glaciated cells) were excluded. Additionally, all cells with no data values in any other remote sensing grid were excluded to train a robust random forest model. The date parameter (day of the year) was implemented to account for the seasonality of the monsoonal regime and seasonal variations in atmospheric conditions in the research area.

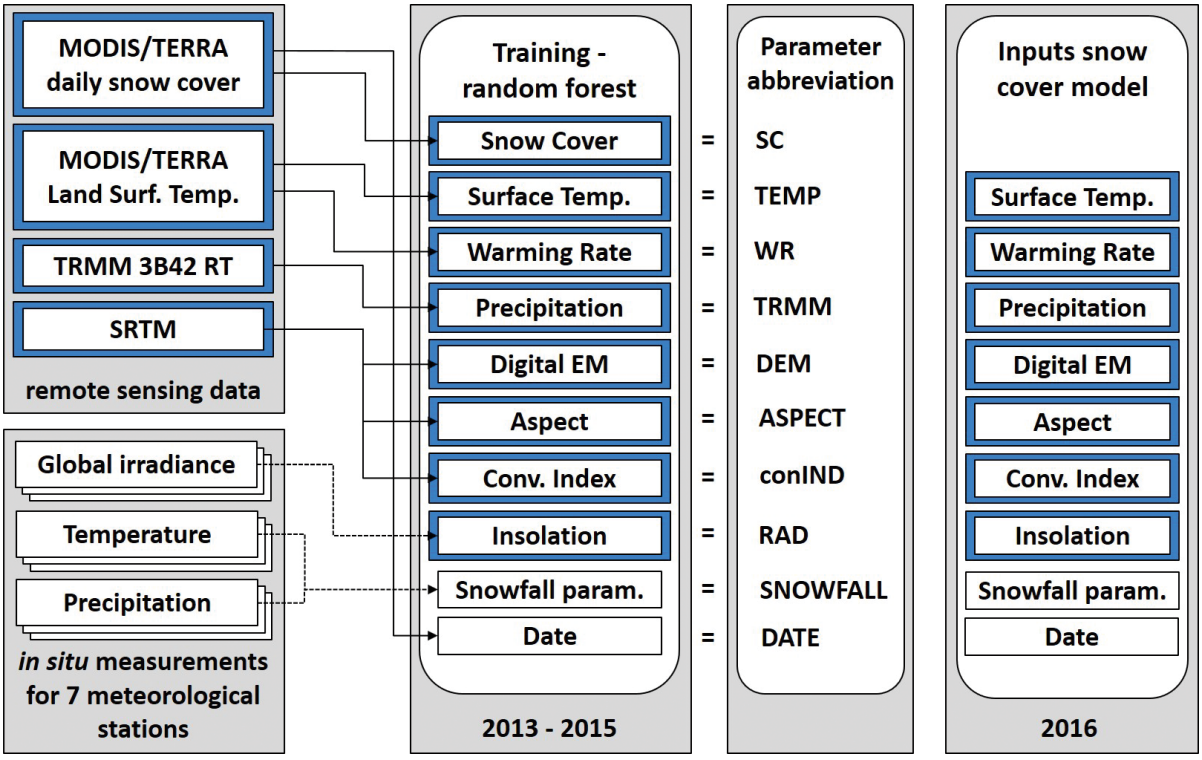

Fig. 2. Delineation of model implementation (Training–random forest), input parameters (remote sensing data and *in situ* measurements), abbreviations and final modelling setup (Inputs snow cover model). EM: elevation model, Conv.: convergence

3.2. Orographic effects and radiation

The Himalayan orogen and the northern adjacent Tibetan Plateau have a large impact on climate, and the mountain belt is a barrier for (moist) monsoonal air masses resulting in very high orographic precipitation (Böhner et al. 2015). The successive mountain ridges are the cause of an intensified lee effect, and thus favour northern shielded areas with higher net shortwave radiation due to reduced cloud cover, higher altitudes and a smaller vertical atmospheric dilation (Böhner 2006). While large-scale gradients between the Indian subcontinent and the Tibetan Plateau are sufficiently resolved in regional climate models or in reanalysis data, small-scale topo-climatic variations are not represented (Gerlitz 2015). To account for these variations, a digital terrain model with an adequate resolution is crucial. Böhner & Antoni (2009) proposed several additional topographic parameters specific to boundary climate processes; however, computing capacity during the modelling process limits the number of additional dimensions for each raster cell. Therefore, a convergence index (radius = 10 raster cells) was calculated in SAGA GIS (Conrad et al. 2015) to identify exposed higher areas and to distinguish these from more protected valley bottoms. Since significant disparity in ablation times of different exposed slopes was observed (and can be expected due to differential incoming shortwave radiation), the aspect parameter with geographic directions was incorporated in the model. Not only direct shortwave insolation, but also diffuse radiation is highly relevant for the micro climate (Domine et al. 2008, Grimm et al. 2013), so the daily global radiation was selected as an additional predictor. Extra-terrestrial solar radiation can be easily calculated using orbital parameters of earth and sun, but actual incoming terrestrial solar radiation is highly dependent on atmospheric and topographic conditions (Böhner et al. 2015). Therefore, several processing steps were applied in order to correct *in situ* measurements of global irradiance and generate spatially complete radiation fields: (1) clearing obvious outliers and measurement errors; (2) generating hourly means and daily totals; (3) calculating daily extra-terrestrial solar radiation for all stations via the R package *SIRAD* (Bojanowski 2015); (4) estimating mean atmospheric transmissivity (Tau) for each day

by normalising observed incoming solar radiation with extra-terrestrial solar radiation; (5) averaging Tau over all stations as input for regionalisation; and (6) calculating incoming solar radiation grids with the help of the sky view factor and shadowing derived from the DEM (Conrad et al. 2015).

3.3. Surface temperatures and warming rates

Among the driving factors for dynamic shifts of snow cover in high mountain areas are near-surface air temperatures. While in general, spatial temperature anomalies are largely explained by underlying elevation, especially at the meso-scale, many overlaying topographic induced factors are vital (Böhner & Antoni 2009, Immerzeel et al. 2009). These are difficult to account for solely by *in situ* measurement, since the distribution and number of the meteorological stations are limited. To maintain necessary spatial temperature model input, daily land surface temperature (LST) data were derived as a substitute from the MODIS/Terra Land Surface Temperatures and Emissivity products (MOD11A1). In addition, this dataset contains night-time LSTs, which allow the calculation of diurnal warming rates (WRs) from the night temperatures of the previous day. WRs provide the advantage of covering swift atmospheric changes, such as sudden clear sky conditions with strong long-wave emissions through the night, and high incoming shortwave radiation on days with less cloud cover or temperature inversions at valley bottoms.

3.4. Precipitation and snowfall

Snowfall is a fundamental input in SDM; however, high spatial robust snowfall estimates are difficult to obtain (Paudel & Andersen 2011, Zhang et al. 2012). To find a sufficient solution for the study period, the TRMM-3B42RT daily precipitation composites (Version 7) were chosen and resampled to the modelling grid. Furthermore, the *in situ* measurements were analysed as well, to add a higher level of endorsement. The meteorological network in the Rolwaling Himal is equipped with tipping rain gauges, which only record fluid depositions but not solid snowfall. The latter is underestimated in principle, as is precipitation during winter months, because the rain gauges are not heated and may freeze (Shrestha et al. 2012; and see www.synotech.de/produkte/datenblatt). Therefore, the *in situ* point measurements are used and a logical (yes/no) snowfall parameterisation is employed. Hereby, suitable conditions, i.e. precipitation and near-surface air temperatures at around 0°C, for potential snow fall are considered.

As shown in Fig. 3a, the MODIS snow cover observations are strongly limited due to clouds. The maximum cloud coverage reaches 94.3% during the observed period. In general, valley slopes and ridges are characterized by high rates of cloud coverage. Lower rates are observed over the valley bottoms, with minimum cloud coverage amounting to 42.9%. This emphasizes the difficulties of accurate high spatio-temporal remote sensing observations in mountain areas. The snow coverage shows a strong

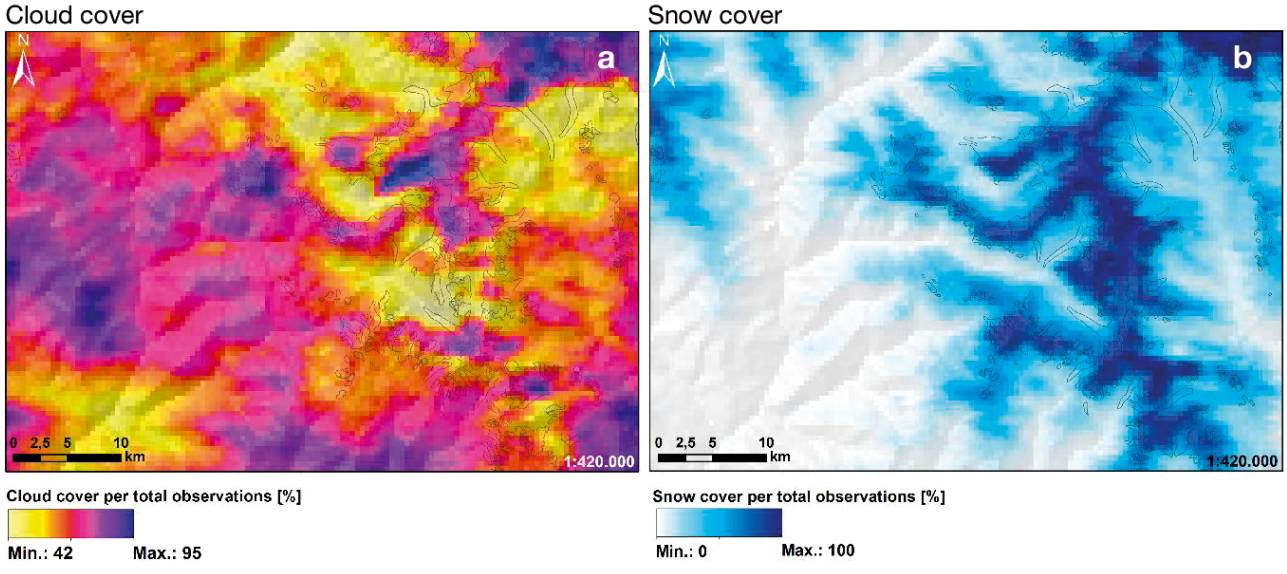

Fig. 3. Days with (a) cloud coverage and (b) snow cover of detected cells during the research period (15 April 2013 to 31 December 2015); data from MODIS (TERRA). Glaciated areas (grey lines) from RGIC (2017)

Table 3. (a) Confusion matrix of predicted (dark grey) and observed classes (light grey), (b) hit rates and class statistics and (c) overall model measurements of the snow distribution model. ***Level of significance >99.99%

(a)

	Snow	Snow-free
Snow	165101	24723
Snow-free	29553	373976

(b)

Class	Hit rates (%)	No. of cells
Snow	86.98	189824
Snow-free	92.69	403529

(c)

Overall accuracy	Kappa
90.85***	0.79

relationship with altitude and aspect throughout the modelling period (Fig. 3b). Highly snow-covered areas only occur above 5000 m a.s.l. South and south-east oriented slopes tend to have a significantly lower snow coverage than north and north-west facing hillsides. This effect is mainly induced by differences between the slopes in incoming solar radiation, and is particularly pronounced in the central Rolwaling valley.

4. RESULTS

4.1. Model performance

The performance of the developed snow distribution model is assessed with several statistical approaches. Although the OOB estimate of error rate in the established random forest is low at 9.22%, the data are split into 80% for training of the random forest model and 20% for the validation. The confusion matrix in Table 3, comparing observed and predicted snow cover, indicates hit rates above 85.0% for both snow-covered and snow-free cells and a highly significant overall model accuracy as well as an unweighted Kappa coefficient of 0.79. The latter was chosen as a performance measure for categorical data because of the high class unbalances within the analysed datasets, resulting in a lower number of snow-covered cells (fewer than 190×10^3) in contrast to snow-free cells with slightly over 400×10^3 (Kuhn 2008).

To assess the model's capacity to provide robust predictions, the winter and pre-monsoon season of 2016 (starting with 1 January 2016) was used to evaluate model performance. This independent evaluation period was excluded from the model set up, and the developed model was run over all days of this evaluation period. For each day, snow-covered and snow-free areas were predicted and compared to the MODIS observations. Overall accuracies (OA) of all predicted cells and unweighted Kappa coefficients are illustrated in Fig. 4 for each day. Both performance measures show an upward trend throughout the independent test season. The missing bars represent 26 days without remote sensing observations on consecutive days. Additionally, 24 days with <10% detected cells in the MODIS snow cover data were excluded to avoid an overfitting in OA due to the class unbalance in favour of snow-free cells, which are thus easier to predict accurately. For the whole test period, the mean OA is 83.7% and the mean Kappa is 0.51.

The comparison of the SDM results for the independent validation period from 2016 with the MODIS observations for different elevation belts shows good performance in general, but a slight underestimation

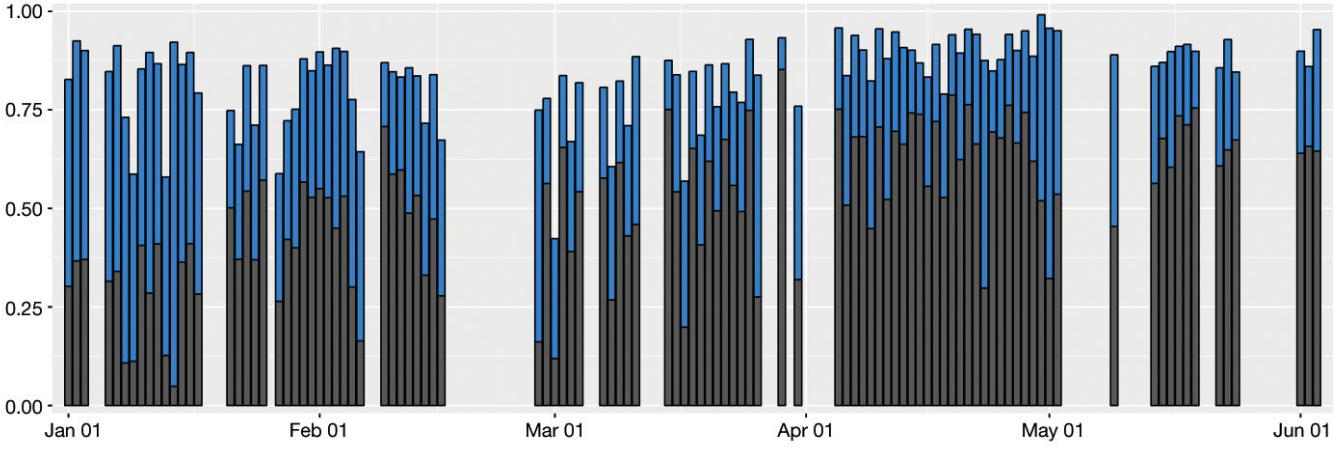

Fig. 4. Overall accuracies (blue) and unweighted Kappa coefficients (grey) from 1 January to 3 June 2016

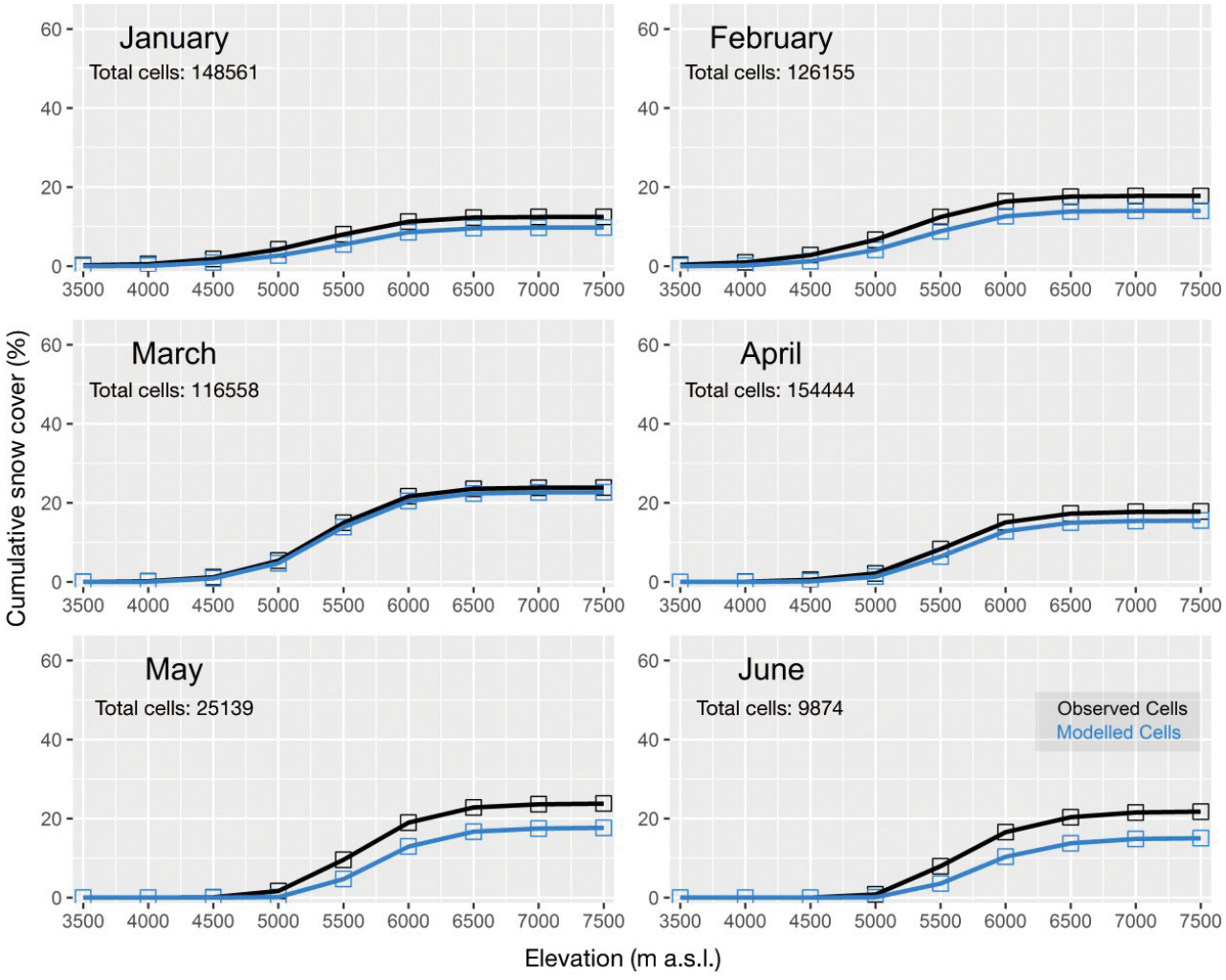

Fig. 5. Cumulative snow cover (%) per month along altitudinal belts in the validation period in 2016

of cumulative snow cover by the model (Fig. 5). Altitudes <3500 m a.s.l. and >7500 m a.s.l. are excluded, as they account for <0.2% of total snow cover during the validation period. Most of the underestimates occur between 4500 and 5500 m a.s.l. throughout the whole period, whereas the best modelling results are found in March and April followed by the least accurate cumulative snow cover in May and June with a deviation of ~5% below the observed snow coverage.

Fig. 6 shows the performance of the SDM for each elevational belt. Only cells with observed snow cover (MODIS) are compared with the modelled cells. The highest altitudes show the best results, with almost always a full representation of snow-covered areas. Below 4500 m a.s.l., there are several days in the 2016 test season which often do not have any snow observations at all from the onset of the pre-monsoon season. For instance, between 3500 and 4000 m a.s.l., snow coverage is completely ablated after March. The following elevational belt shows a strong reduction of snow cover after April, clearly representing the seasonal cycle of the snow line. This is well captured by the modelling results. Nevertheless, in the lower belts, snow coverage is detected by MODIS but is not accurately resolved in the model for several days. As demonstrated in Fig. 4, these lower-located cells only have a minor share of total snow coverage.

4.2. Sensitivity analysis

The most relevant variables driving the model are shown in Fig. 7. The analysis of the MDA indicates the seasonality proxy DATE as the main input parameter with the largest potential loss in model accuracy if left out, followed by remote sensing de-

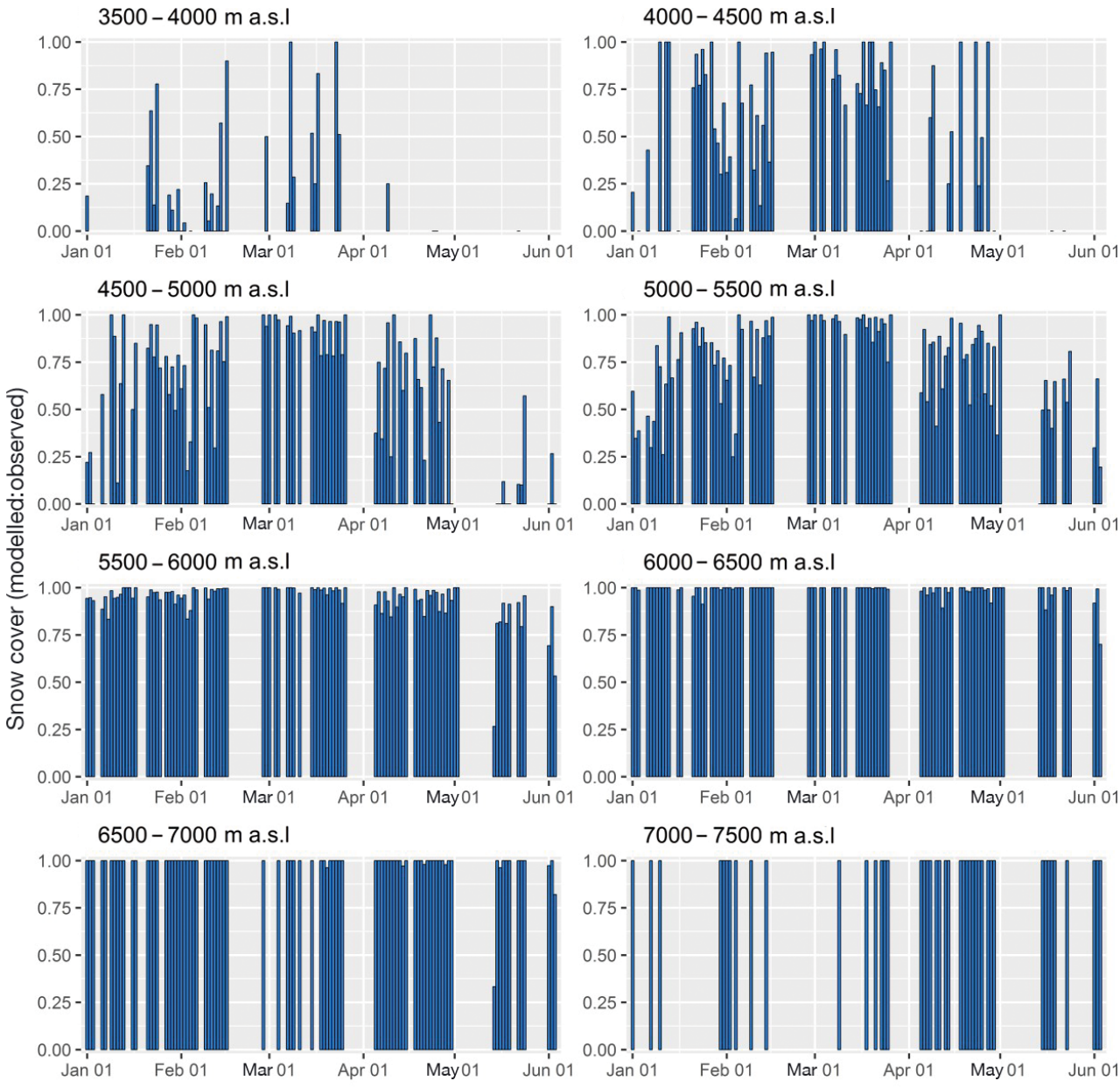

Fig. 6. Ratios of modelled vs. observed snow cover during the independent evaluation season (January–June) in 2016 for elevational belts from 3500 up to 7500 m a.s.l.

rived rainfall estimates (TRMM) and LSTs (TEMP). Subsequently, all variables related to the local topography are of importance. High MDA values are detected for insolation (RAD) and the convergence index (ConIND) followed by elevation (DEM) and slope exposition (ASPECT). The WR and snowfall indicator (SNOWFALL) tend to have lesser relevance for the model, caused by the simplified snow parameterisation and the strong dependencies between monsoonal seasonality, nocturnal LSTs and daytime LSTs already implemented in previous inputs (Ishwaran 2007). Based on the MDI, LSTs (TEMP) are of importance to form nodes with homogenous snow cover characteristics. LSTs are followed by elevation (DEM) and the seasonality indicator DATE. This demonstrates that the model's ability to classify each cell accurately over the whole heterogeneous research domain is mainly based on these 3 input variables. Particularly for the transition area of classification, ConIND, WR, RAD and ASPECT show an added value, although for most of the cells they do not provide any useful information. The lowest MDI is found

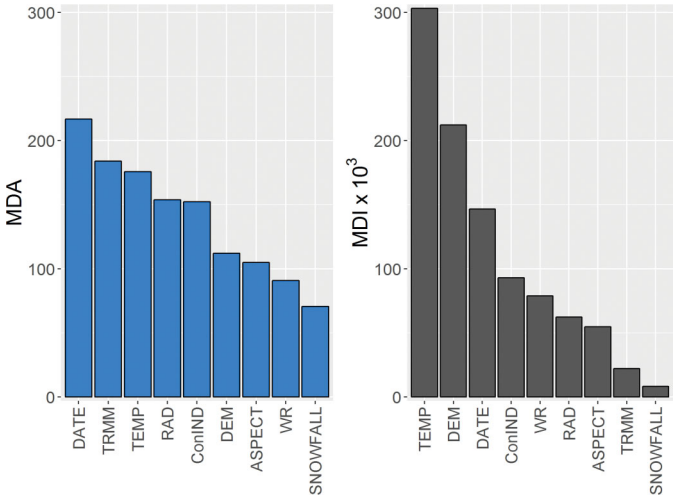

Fig. 7. Mean decrease in accuracy (MDA) and mean decrease in impurity (MDI) of the snow distribution model. Abbreviations as in Fig. 2

for remotely sensed rainfall estimates TRMM and SNOWFALL.

In order to evaluate the response of the statistical model, a sensitivity analysis is shown in Fig. 8. Here variations of all input parameters regarding their MDI ranks are displayed (the TRMM and the SNOWFALL parameter are excluded due to their poor ability to reduce node impurities of the random forest). The reference snow-covered area under mean conditions (centre column Fig. 8 and black outlines in the neighbouring maps) is given in each row to compare the changes in snow cover by deducted (left column) and added (right column) standard deviations. The LSTs (TEMP) have the strongest influence on the model results, followed by the elevation (DEM). The MDI ranking is consistent with the provided sensitivity analysis, except the topographic exposure to wind (ConIND), which has no clear visible impact on the spatial snow cover distribution.

4.3. Clear sky validation days

To visualize the model's capacity to accurately map snow cover dynamics in high mountain regions, 2 days of the test period were spatially analysed. In Fig. 9, a snow recession event occurring from 9 to 10 February 2016 is shown to demonstrate the SDM's capacity to predict snow cover dynamics at high spatial resolution and on a daily scale. Both days show high prediction accuracies with 87.0 and 84.7 % for 9 and 10 February, respectively. Nevertheless, on both days the SDM's minor underestimation of snow cover is visible. Visually there is a high agreement between the SDM's predictions and the MODIS observations, which is supported by unweighted Kappa values of 0.71 (9 February) and 0.60 (10 February). The model forms a rather cohesive snow line, but still predicts sheltered snow-free areas within the mountain range (9 February, central-north). Lower elevated slopes and valley bottoms are adequately predicted as snow free in both example days. The snow-covered areas are well represented, although some minor deviations are found. For instance, snow patches on 9 February along the slopes of the central Tama Koshi valley are very heterogeneous, whereas the predicted snow cover edge is rather abrupt. The brighter cells in the SDM prediction represent modelled cell characteristics for cloud covered cells in the original MODIS product. As the figures show, our approach is able to close data gaps in the MODIS snow cover products. Compared to the observations, the SDM has a higher average information content of 6.6 % (9 and 10 February 2016).

5. DISCUSSION

The performance of the presented statistical snow distribution model is comparable to physical top-down approaches. Shrestha et al. (2012) applied a distributed hydrological model containing a 3-layer energy-balance snow physics module to the Khumbu Himal region and achieved a mean overall accuracy in predicting snow cover correctly of approximately 90 % compared to the MODIS 8 d composite snow cover product (MOD10A2). As the Khumbu Himal is very close to the Rolwaling Himal, it is well suited for comparison. In addition, in contrast to Shrestha et al. (2012), the monsoon months were taken into account, which are more challenging in terms of both observation and modelling. High cloud coverages, low snow detection rates by MODIS and an elevated orographic snow line only provide a limited set of training data during the monsoon (Gao et al. 2010). Thus, reliable inputs for statistical modelling are not equally available during all seasons, which leads to different levels of modelled snow cover quality throughout the seasons. Nevertheless, hit rates and presented seasonal analysis fortify proper model behaviour.

We found the accuracy of modelled snow cover to be around 91 % for the SDM (Table 3). Considering the lower error rate and the lesser cloud coverage in the 8 d MODIS composites used by Shrestha et al. (2015), a better performance can be assumed due to better model calibration conditions compared to the

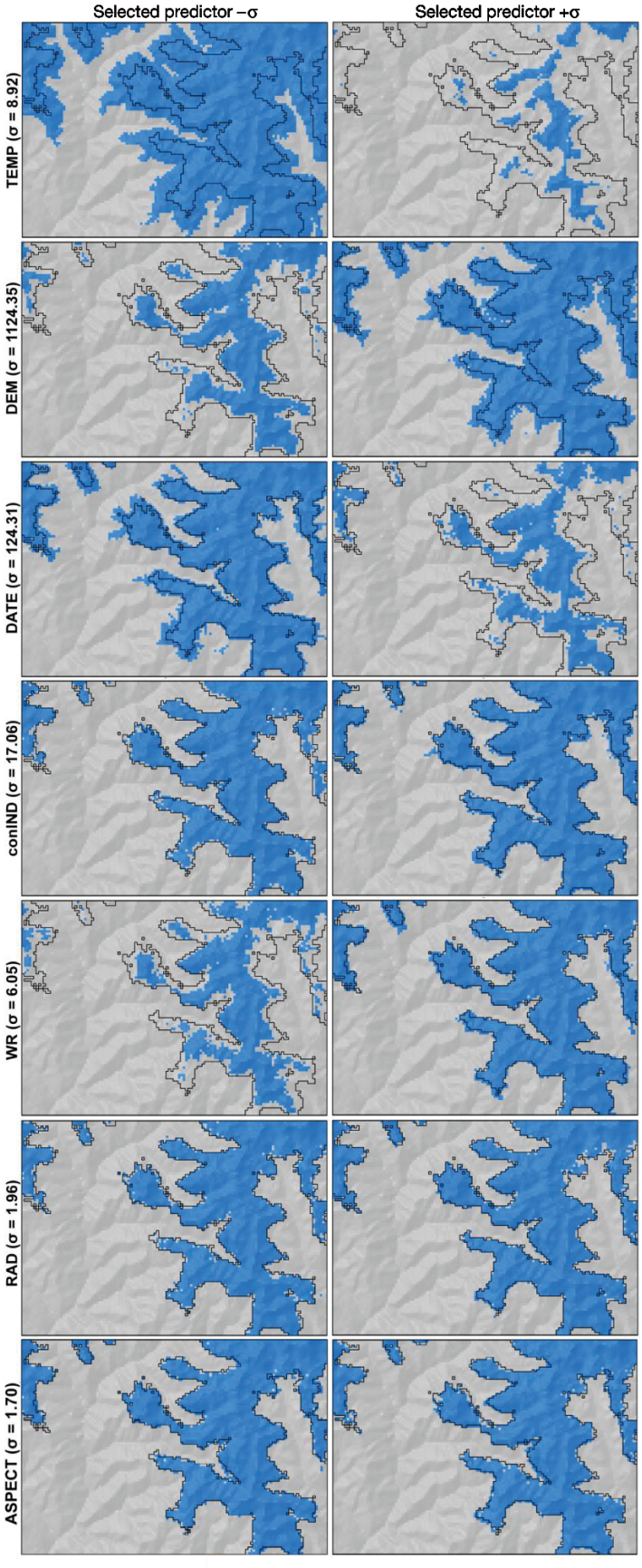

Fig. 8. Sensitivity analysis according to mean decrease in impurity (MDI; above 50×10^3) values and their effect on mean cell values of all inputs (for snowfall, the mode of each cell is used). In each row, only the parameter headed is altered from the mean cell values, where the left column shows a negative offset of each cell with the overall standard deviation (−σ) of all training data and the right column shows a positive deviation (+σ). Black lines: model output for means of all parameters for each individual cell

daily snow cover product implemented in our approach (Tekeli et al. 2005). The very high correlation of cumulative snow cover over altitudinal belts with the observed snow distribution during the winter and pre-monsoon season (Fig. 5) can partly be explained with the availability of training data for the random forest. The superior atmospheric conditions allow a higher number of actual observations (e.g. March with 116 558 compared to May with 25 139) by all dynamic remote sensing products (Table 2). This larger number of observations permits the random forest to represent the snow distribution much more accurately for months in the winter, pre- and post-monsoon season. While the elevational distribution of snow coverage in May and June is still adequately resolved, the error rate especially at altitudes below 4500 m a.s.l. (Fig. 6) is high during these months. Nevertheless, the limited data coverage and a larger detection error in MODIS snow cover products leads to a lower model accuracy during the summer monsoon season (Paudel & Andersen 2011, Shrestha et al. 2012). Therefore, a larger research domain and a temporal weighted input selection is a promising way for further enhancements, particularly with regard to an extension of the training data set.

In contrast to other studies, which suggested a combination of snow cover with both MODIS platforms, TERRA and AQUA (Rodell & Houser 2004, Gao et al. 2010, Paudel & Andersen 2011, Rittger et al. 2013), the inclusion of AQUA data did not improve our results. This might partly result from the large temporal difference in satellite orbits and overpass times (approximately 3 h, e.g. 17 April 2013, TERRA 11:30 h and AQUA 14:40 h local time GMT+05:45, for the research domain) between both platforms.

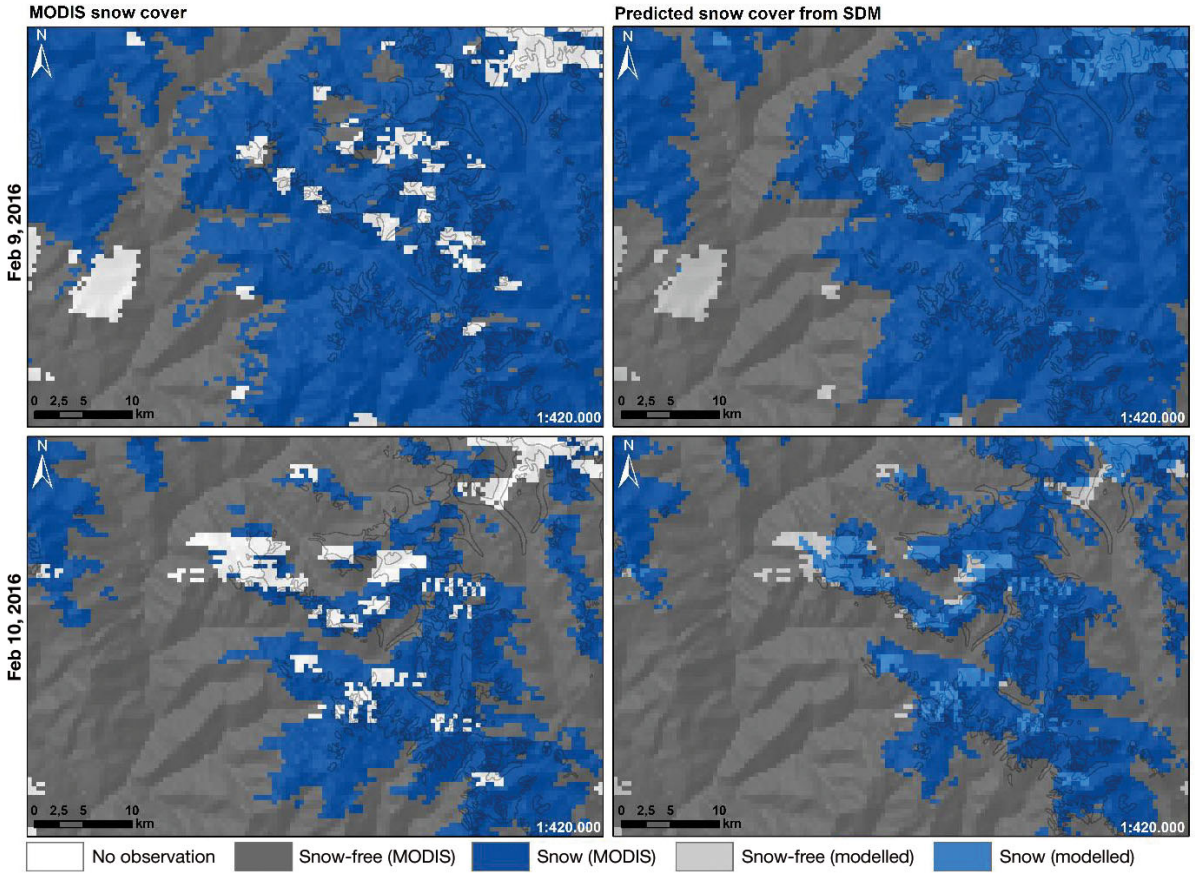

Fig. 9. Snow recession event during February 2016 with MODIS observations (left) and snow distribution modelling (SDM) results (right). Light grey (snow-free) and light blue (snow-covered) cells on the right side are the modelled surface characteristics where no observation was available from MODIS. Glaciated areas from RGIC (2017)

This leads to strong dissimilarities in actual snow coverage in the Rolwaling Himal. The fast snow depletion at southern and eastern slopes from sunrise till noon potentially ablates minor snow layers of only a few centimeters between the 2 overpasses, and introduces a substantial source of error in combining both platforms.

Although the accurate prediction of snow cover at higher altitudes (>5500 m a.s.l.) is less challenging than close to the snow line elevation, the modelling approach is very accurate over time in these areas (Fig. 6). The seasonal variability of the orographic snow line is traceable up to 5500–6000 m a.s.l., where it is apparent at the beginning of April and even up to 6000–6500 m a.s.l., at the beginning of May. Thus, the developed modelling approach is capable of accurately predicting snow cover distributions at a daily resolution.

Besides our modelling focus, the binary snow cover, there are several other important snow parameters, such as snow water equivalent (SWE) or snow cover fractions. These are of special interest, as they contain more information on snow conditions, and in case of SWEs are crucial inputs for hydrological applications. Nevertheless, data availability, data quality and spatio-temporal resolutions are limited (Zhang et al. 2012, Shrestha et al. 2015). Thus, for our statistical approach, we decided to investigate the basic snow cover derived by MODIS.

The sensitivity analysis emphasizes the hierarchical model structure as indicated by the MDIs of all input parameters. The highest influence of the TEMP parameter is visually traceable for both directions of the standard deviations (Fig. 8), followed by the elevation (DEM). Each split of each single tree of the random forest might have unique threshold values for the cell classification due to bagging. The modelling approach is able to capture non-linear relationships and variable interactions. Thus, asymmetrical snow cover distributions can occur for positive and negative deviations of the considered input parameters. This is, for example, the case for intraday WRs, where reduced WRs show a strong effect on the snow cover distribution, whereas no effect could be de-

tected for positive anomalies. The maximum WRs (between night and daytime) occur on snow-free rock surfaces on southerly slopes (ASPECT) due to high nocturnal radiative cooling and a steep rise in surface temperatures during daytime due to solar insolation. Lower warming rates occur during monsoon because of high rates of cloud coverage during the night (Domine et al. 2008, Engel et al. 2017). Therefore, lower warming rates can be an indicator for snow melt, which is adequately represented in the sensitivity analysis (Fig. 8, row 5). The sensitivity of the seasonality parameter (DATE) reveals the importance of topographical parameters for snow distribution modelling in a high mountain environment. For instance, lowered DATE cell mean values show a correlation with an increased snow cover on north- and northwest-facing slopes (ASPECT) but stable conditions in all other parts. High mountain ridges are characterized by shadowing effects on north-facing slopes, which protects snow patches from melting and sublimation.

The convergence index (ConIND) shows great relevance in either MDAs and MDIs, but only minor changes within the sensitivity analysis (Fig. 8). A static topographic parameter has the highest influence at the minimum −35.0 (sheltered valley bottoms) and at the maximum +35.0 (mountain tops exposed to strong winds). Therefore, smaller changes around the mean without the combination of other variables have almost no effects on the modelling. The static exposure parameter (ASPECT) influences the lower elevated north-facing slopes, where it shows the highest influences in the sensitivity analysis. Again, shadowing and incoming solar radiation contribute to this effect.

Although the TRMM parameter provides the second lowest MDI, it is important for the modelling accuracy constrained by the second highest MDAs. Because of its coarse spatial resolution with ca. 27.8 × 27.8 km^2, it only contributes limited information to the model, with its low spatial variance for each day. However, in combination with other inputs in earlier splits of the random forest, such as DATE, it enables the model to accurately predict cells with no clear tendency. Thus, according to the MDAs, TRMM has the highest loss of model accuracy, if left out. An important factor for snow cover modelling is the land cover type (Zaitchik & Rodell 2009, Shrestha et al. 2015). However, as cover types were already used during pre-processing for MODIS LSTs and snow cover, they were not included during this modelling setup, to avoid multicollinearities (Riggs et al. 2006).

Considering the model input variables, development of a setup consisting solely of remote sensing and topographic products is currently in progress, as only the global irradiance values add a significant additional benefit towards the model's performance, whereas the snowfall parameterisation is the least important input as demonstrated in the sensitivity analysis. However, a minor decrease in quality is expected, since atmospheric transmission has to be compensated with additional remote sensing products, for instance the MODIS MOD05_L2 column water-vapour amount products or MOD06_L2 with cloud cover fractions.

6. CONCLUSIONS

Prior work has documented the feasibility of physical top-down approaches to model snow cover and snow-related parameters in high mountain regions of the Himalayas. These are basically implemented in comprehensive hydrological models, such as GEOtop 2.0 (Endrizzi et al. 2014). Due to the fundamental impacts and feedbacks of snow (cover) in high mountain environments, such as changes in albedo and water storage, as well as protection for soil and biota, information about snow properties is crucial to multiple scientific interests (Berrisford et al. 2009, Immerzeel et al. 2009). However, these physically based modelling approaches or reanalysis datasets have shortcomings in spatial and/or temporal resolution.

The focus of this study was to evaluate the performance of a prevalent machine learning algorithm, a random forest, trained with daily MODIS snow cover maps in order to decrease known deficits in top-down approaches and provide a computationally extensive, statistically robust and transferable method to predict snow cover in the Central Himalayan region. This survey found strong relationships and dependencies between spatio-temporal climatic variations, topographic parameters and snow cover dynamics. The presented model's capacity to predict daily snow distributions accurately on a 500 × 500 m raster grid throughout winter, pre- and post-monsoon seasons shows a sound conformity with state-of-the-art approaches. Compared to Shrestha et al. (2012), the present method achieved slightly better performances in model accuracy, with 90.85% (compared to 90.0%) and had a higher temporal resolution (daily vs. 8 d evaluation). The main physical processes regarding snow cover dynamics are reproducible with a training data set covering around 3 years of meteorological data and remote sensing observations combined with GIS-derived topographical parameters.

Acknowledgements. We are very grateful to local guides and Sherpa, especially Tenzin Sherpa and Dawa Chhiri Sherpa, who accompanied us on numerous field trips to our climate stations. The modelling approach is embedded in the framework of the TREELINE project and partially funded by the German Research Foundation (DFG, GZ: BO 1333/4-1, SCHI 436/14-1) as well as the Cluster of Excellence CliSAP (EXC177). Additionally, we thank the 3 anonymous reviewers for their insightful comments and thoughts on an earlier version of the manuscript.

LITERATURE CITED

Alford D, Armstrong R (2010) The role of glaciers in stream flow from the Nepal Himalaya. Cryosph Discuss 4: 469–494

Anders AM, Roe GH, Hallet B, Montgomery DR, Finnegan NJ, Putkonen J (2006) Spatial patterns of precipitation and topography in the Himalaya. Geol Soc Am Spec Pap 398:39–53

Apel H, Abdykerimova Z, Agalhanova M, Baimaganbetov A and others (2018) Statistical forecast of seasonal discharge in Central Asia for water resources management: Development of a generic linear modelling tool for operational use. Hydrol Earth Syst Sci 22:2225–2254

Auer AH Jr (1974) The rain versus snow threshold temperatures. Weatherwise 27:67

Bechtel B, Daneke C (2012) Classification of local climate zones based on multiple earth observation data. IEEE J Sel Top Appl Earth Obs Remote Sens 5:1191–1202

Belgiu M, Drăguţ L (2016) Random forest in remote sensing: a review of applications and future directions. ISPRS J Photogramm Remote Sens 114:24–31

Berrisford P, Dee D, Fielding K, Fuentes M, Kallberg P, Kobayashi S, Uppala S (2009) The ERA-interim archive. ERA Rep Ser 1:1–16

Biau G (2012) Analysis of a random forests model. J Mach Learn Res 13:1063–1095

Blöschl G, Kirnbauer R, Gutknecht D (1991) Distributed snowmelt simulations in an alpine catchment. 1. Model evaluation on the basis of snow cover patterns. Water Resour Res 27:3171–3179

Böhner J (2006) General climatic controls and topoclimatic variations in Central and High Asia. Boreas 35:279–295

Böhner J, Antonić O (2009) Land-surface parameters specific to topo-climatology. Dev Soil Sci 33:195–226

Böhner J, Miehe G, Meihe S, Nagy L (2015) Climate and weather. In: Miehe G, Pendry C, Chaudhary RP (eds) Nepal. An introduction to the natural history, ecology and human environment of the Himalayas. A companion to the Flora of Nepal. Royal Botanic Garden Edinburgh, p 23–90

Bojanowski JS (2015) sirad: functions for calculating daily solar radiation and evapotranspiration

Bokhorst S, Pedersen SH, Brucker L, Anisimov O and others (2016) Changing Arctic snow cover: a review of recent developments and assessment of future needs for observations, modelling, and impacts. Ambio 45:516–537

Braithwaite RJ (1995) Positive degree-day factors for ablation on the Greenland ice sheet studied by energy-balance modelling. J Glaciol 41:153–160

Breiman L (2001) Random forests. Mach Learn 45:5–32

Breiman L (2002) Manual on setting up, using, and understanding random forests v3. 1. Statistics Department, University of California Berkeley, CA

Breiman L, Friedman J, Stone CJ, Olshen RA (1984) Classification and regression trees. CRC Press, Boca Raton, FL

Brun E, Vionnet V, Boone A, Decharme B and others (2013) Simulation of northern Eurasian local snow depth, mass, and density using a detailed snowpack model and meteorological reanalyses. J Hydrometeorol 14:203–219

Carlson BZ, Choler P, Renaud J, Dedieu JP, Thuiller W (2015) Modelling snow cover duration improves predictions of functional and taxonomic diversity for alpine plant communities. Ann Bot (Lond) 116:1023–1034

Chen IC, Hill JK, Ohlemüller R, Roy DB, Thomas CD (2011) Rapid range shifts of species associated with high levels of climate warming. Science 333:1024–1026

Clyde GD (1931) Snow-melting characteristics. Utah Agric Exp Stn Bull 231:1–23

Cohen J (1960) A coefficient of agreement for nominal scales. Educ Psychol Meas 20:37–46

Conrad O, Bechtel B, Bock M, Dietrich H and others (2015) System for automated geoscientific analyses (SAGA) v. 5.0.0. Geosci Model Dev 8:1991–2007

Dawson CW, Wilby RL (2001) Hydrological modelling using artificial neural networks. Prog Phys Geogr 25:80–108

Dinku T, Connor SJ, Ceccato P (2010) Comparison of CMORPH and TRMM-3B42 over mountainous regions of Africa and South America. In: Gebremichael M, Hossain F (eds) Satellite rainfall applications for surface hydrology. Springer, Dordrecht, p 193–204

Domine F, Albert M, Huthwelker T, Jacobi HW and others (2008) Snow physics as relevant to snow photochemistry. Atmos Chem Phys 8:171–208

Durand M, Kim EJ, Margulis SA (2009) Radiance assimilation shows promise for snowpack characterization. Geophys Res Lett 36:L02503

Endrizzi S, Gruber S, Dall'Amico M, Rigon R (2014) GEOtop 2.0: simulating the combined energy and water balance at and below the land surface accounting for soil freezing, snow cover and terrain effects. Geosci Model Dev 7: 2831–2857

Engel M, Notarnicola C, Endrizzi S, Bertoldi G (2017) Snow model sensitivity analysis to understand spatial and temporal snow dynamics in a high-elevation catchment. Hydrol Processes 31:4151–4168

Essery R (1999) Parametrization of heterogeneous snowmelt. Theor Appl Climatol 62:25–30

Forman BA, Reichle RH, Rodell M (2012) Assimilation of terrestrial water storage from GRACE in a snow-dominated basin. Water Resour Res 48:W01507

Franz KJ, Karsten LR (2013) Calibration of a distributed snow model using MODIS snow covered area data. J Hydrol (Amst) 494(Suppl C):160–175

Gao J, Williams MW, Fu X, Wang G, Gong T (2012) Spatiotemporal distribution of snow in eastern Tibet and the response to climate change. Remote Sens Environ 121: 1–9

Gao W, Kafatos M, Murphy RE, Salomonson VV (2006) Earth science satellite remote sensing: science and instruments. Springer, Berlin

Gao Y, Xie H, Lu N, Yao T, Liang T (2010) Toward advanced daily cloud-free snow cover and snow water equivalent products from Terra–Aqua MODIS and Aqua AMSR-E measurements. J Hydrol (Amst) 385:23–35

Genuer R, Poggi JM, Tuleau-Malot C (2010) Variable selection using random forests. Pattern Recognit Lett 31: 2225–2236

Gerlitz L (2015) Using fuzzified regression trees for statistical downscaling and regionalization of near surface temperatures in complex terrain. Theor Appl Climatol 122: 337–352

Gerlitz L, Conrad O, Böhner J (2015) Large-scale atmospheric forcing and topographic modification of precipitation rates over High Asia — a neural-network-based approach. Earth Syst Dyn 6:61–81

Gerlitz L, Bechtel B, Böhner J, Bobrowski M and others (2016a) Analytic comparison of temperature lapse rates and precipitation gradients in a Himalayan treeline environment: implications for statistical downscaling. In: Singh R, Schickhoff U, Mal S (eds) Climate change, glacier response, and vegetation dynamics in the Himalaya. Springer, Cham, p 49–64

Gerlitz L, Vorogushyn S, Apel H, Gafurov A, Unger-Shayesteh K, Merz B (2016b) A statistically based seasonal precipitation forecast model with automatic predictor selection and its application to central and south Asia. Hydrol Earth Syst Sci 20:4605–4623

Grabherr G, Gottfried M, Pauli H (2010) Climate change impacts in alpine environments. Geogr Compass 4: 1133–1153

Grimm NB, Chapin FS III, Bierwagen B, Gonzalez P and others (2013) The impacts of climate change on ecosystem structure and function. Front Ecol Environ 11:474–482

Hall DK, Riggs GA, Salomonson VV (1995) Development of methods for mapping global snow cover using moderate resolution imaging spectroradiometer data. Remote Sens Environ 54:127–140

Hall DK, Riggs GA, Salomonson VV, DiGirolamo NE, Bayr KJ (2002) MODIS snow-cover products. Remote Sens Environ 83:181–194

He ZH, Parajka J, Tian FQ, Blöschl G (2014) Estimating degree-day factors from MODIS for snowmelt runoff modeling. Hydrol Earth Syst Sci 18:4773–4789

Hernández-Henríquez MA, Déry SJ, Derksen C (2015) Polar amplification and elevation-dependence in trends of Northern Hemisphere snow cover extent, 1971–2014. Environ Res Lett 10:044010

Hiemstra CA, Liston GE, Reiners WA (2006) Observing, modelling, and validating snow redistribution by wind in a Wyoming upper treeline landscape. Ecol Model 197: 35–51

Hock R (2003) Temperature index melt modelling in mountain areas. J Hydrol (Amst) 282:104–115

Hoinkes HC, Steinacker R (1975) Hydrometeorological implications of the mass balance of Hintereisferner, 1952–53 to 1968–69. IAHS Publ 104:144–149

Houborg R, Rodell M, Li B, Reichle R, Zaitchik BF (2012) Drought indicators based on model-assimilated Gravity Recovery and Climate Experiment (GRACE) terrestrial water storage observations. Water Resour Res 48:W07525

Huffman GJ, Bolvin DT, Nelkin EJ, Wolff DB and others (2007) The TRMM multisatellite precipitation analysis (TMPA): quasi-global, multiyear, combined-sensor precipitation estimates at fine scales. J Hydrometeorol 8: 38–55

Immerzeel WW, Droogers P, Jong SM, Bierkens MFP (2009) Large-scale monitoring of snow cover and runoff simulation in Himalayan river basins using remote sensing. Remote Sens Environ 113:40–49

Immerzeel WW, Petersen L, Ragettli S, Pellicciotti F (2014) The importance of observed gradients of air temperature and precipitation for modeling runoff from a glacierized watershed in the Nepalese Himalayas. Water Resour Res 50:2212–2226

Ishwaran H (2007) Variable importance in binary regression trees and forests. Electron J Stat 1:519–537

Jarvis A, Reuter HI, Nelson A, Guevara E (2008) Hole-filled seamless SRTM data V4. Tech Rep. International Centre for tropical Agriculture (CIAT), Cali. http://srtm.csi.cgiar.org

Jeníček M, Beitlerová H, Hasa M, Kučerová D, Pevná H, Podzimek S (2012) Modelling snow accumulation and snowmelt runoff: present approaches and results. AUC Geographica 47:15–24

Kuhn M (2008) Caret package. J Stat Softw 28:1–26

Kwon Y, Yang ZL, Zhao L, Hoar TJ, Toure AM, Rodell M (2016) Estimating snow water storage in North America using CLM4, DART, and snow radiance data assimilation. J Hydrometeorol 17:2853–2874

Kwon Y, Yang ZL, Hoar TJ, Toure AM (2017) Improving the radiance assimilation performance in estimating snow water storage across snow and land-cover types in North America. J Hydrometeorol 18:651–668

Liaw A, Wiener M (2002) Classification and regression by randomForest. R News 2:18–22

Liston GE, Elder K (2006) A distributed snow-evolution modeling system (SnowModel). J Hydrometeorol 7: 1259–1276

Litaor MI, Williams M, Seastedt TR (2008) Topographic controls on snow distribution, soil moisture, and species diversity of herbaceous alpine vegetation, Niwot Ridge, Colorado. J Geophys Res 113:G02008

Loth B, Graf HF (1988) Modeling the snow cover in climate studies. 1. Long-term integrations under different climatic conditions using a multilayered snow-cover model. J Geophys Res 103:11313–11327

Louppe G, Wehenkel L, Sutera A, Geurts P (2013) Understanding variable importances in forests of randomized trees. In: Burges CJC, Botton L, Welling M, Grahamani Z, Weinberger KQ (eds) Proc Adv Neural Inf Processing Syst, December 5, 2013, Lake Tahoe, NV, p 431–439

Marks D, Domingo J, Susong D, Link T, Garen D (1999) A spatially distributed energy balance snowmelt model for application in mountain basins. Hydrol Processes 13: 1935–1959

Martinec J, Rango A, Roberts R (2008) Snowmelt runoff model (SRM) user's manual. Updated edition for Windows. WinSRM Version 1.11. http://aces.nmsu.edu/pubs/research/weather_climate/SRMSpecRep100.pdf

Panday PK, Williams CA, Frey KE, Brown ME (2014) Application and evaluation of a snowmelt runoff model in the Tamor River basin, Eastern Himalaya using a Markov Chain Monte Carlo (MCMC) data assimilation approach. Hydrol Processes 28:5337–5353

Paudel KP, Andersen P (2011) Monitoring snow cover variability in an agropastoral area in the Trans Himalayan region of Nepal using MODIS data with improved cloud removal methodology. Remote Sens Environ 115: 1234–1246

Pedersen VK, Egholm DL (2013) Glaciations in response to climate variations preconditioned by evolving topography. Nature 493:206–210

Prasad AM, Iverson LR, Liaw A (2006) Newer classification and regression tree techniques: bagging and random forests for ecological prediction. Ecosystems 9:181–199

Pu Z, Xu L, Salomonson VV (2007) MODIS/Terra observed seasonal variations of snow cover over the Tibetan

Plateau. Geophys Res Lett 34:L06706
Putkonen JK (2004) Continuous snow and rain data at 500 to 4400 m altitude near Annapurna, Nepal, 1999–2001. Arct Antarct Alp Res 36:244–248
Rastner P, Irsara L, Schellenberger T, Della Chiesa S and others (2009) Snow cover monitoring and modelling in the Alps using multi temporal MODIS data. Proc Int Snow Sci Workshop, Davos 2009, p 214–218
R Core Team (2014) R: a language and environment for statistical computing. R Foundation for Statistical Computing, Vienna
RGIC (Randolph Glacier Inventory Consortium) (2017) Randolph Glacier Inventory 6.0. https://www.glims.org/RGI/
Riggs GA, Hall DK, Salomonson VV (2006) MODIS snow products user guide to collection 5. Digit Media 80. https://modis-snow-ice.gsfc.nasa.gov/uploads/sug_c5.pdf
Rittger K, Painter TH, Dozier J (2013) Assessment of methods for mapping snow cover from MODIS. Adv Water Resour 51:367–380
Rodell M, Houser PR (2004) Updating a land surface model with MODIS-derived snow cover. J Hydrometeorol 5: 1064–1075
Rohrer M, Salzmann N, Stoffel M, Kulkarni AV (2013) Missing (in-situ) snow cover data hampers climate change and runoff studies in the Greater Himalayas. Sci Total Environ 468–469(Suppl):S60–S70
RStudio Team (2015) RStudio: integrated development for R. RStudio, Inc., Boston, MA
Schickhoff U, Bobrowski M, Böhner J, Bürzle B and others (2015) Do Himalayan treelines respond to recent climate change? An evaluation of sensitivity indicators. Earth Syst Dyn 6:245–265
Schwab N, Schickhoff U, Bürzle B, Hellmold J, Stellmach M (2015) Dendroecological studies in the Nepal Himalaya–review and outlook in the context of a new research initiative (TREELINE). TRACE 13:86–95
Shrestha M, Wang L, Koike T, Xue Y, Hirabayashi Y (2012) Modeling the spatial distribution of snow cover in the Dudhkoshi region of the Nepal Himalayas. J Hydrometeorol 13:204–222
Shrestha M, Koike T, Hirabayashi Y, Xue Y, Wang L, Rasul G, Ahmad B (2015) Integrated simulation of snow and glacier melt in water and energy balance-based, distributed hydrological modeling framework at Hunza River Basin of Pakistan Karakoram region. J Geophys Res Atmos 120:4889–4919
Sirguey P, Mathieu R, Arnaud Y (2009) Subpixel monitoring of the seasonal snow cover with MODIS at 250 m spatial resolution in the Southern Alps of New Zealand: methodology and accuracy assessment. Remote Sens Environ 113:160–181
Soria-Auza RW, Kessler M, Bach K, Barajas-Barbosa PM, Lehnert M, Herzog SK, Böhner J (2010) Impact of the quality of climate models for modelling species occurrences in countries with poor climatic documentation: a case study from Bolivia. Ecol Model 221:1221–1229
Stanzel P, Haberl U, Nachtnebel HP (2008) Modelling snow accumulation and snow melt in a continuous hydrological model for real-time flood forecasting. IOP Conf Ser Earth Environ Sci 4:012016
Stieglitz M, Ducharne A, Koster R, Suarez M (2001) The impact of detailed snow physics on the simulation of snow cover and subsurface thermodynamics at continental scales. J Hydrometeorol 2:228–242
Stocker TF, Qin D, Plattner GK, Tignor M and others (eds) (2013) Climate change 2013: the physical science basis. Contribution of Working Group I to the Fifth Assessment Report of the Intergovernmental Panel on Climate Change. Cambridge University Press, Cambridge
Strobl C, Boulesteix AL, Zeileis A, Hothorn T (2007) Bias in random forest variable importance measures: illustrations, sources and a solution. BMC Bioinformatics 8:25
Strobl C, Boulesteix AL, Kneib T, Augustin T, Zeileis A (2008) Conditional variable importance for random forests. BMC Bioinformatics 9:307
Tekeli AE, Akyürek Z, Şorman AA, Şensoy A, Şorman AÜ (2005) Using MODIS snow cover maps in modeling snowmelt runoff process in the eastern part of Turkey. Remote Sens Environ 97:216–230
Timofeev R (2004) Classification and regression trees (CART) theory and applications. MA thesis, Humboldt University, Berlin
Trnka M, Kocmánková E, Balek J, Eitzinger J and others (2010) Simple snow cover model for agrometeorological applications. Agric For Meteorol 150:1115–1127
Vesterdal L, Clarke N, Sigurdsson BD, Gundersen P (2013) Do tree species influence soil carbon stocks in temperate and boreal forests? For Ecol Manag 309:4–18
Wan Z (2006) MODIS land surface temperature products users' guide. Institute for Computational Earth System Science, University of California, Santa Barbara, CA
Wan Z, Dozier J (1996) A generalized split-window algorithm for retrieving land-surface temperature from space. IEEE Trans Geosci Remote Sens 34:892–905
Wang W, Huang X, Deng J, Xie H, Liang T (2015) Spatio-temporal change of snow cover and its response to climate over the Tibetan Plateau based on an improved daily cloud-free snow cover product. Remote Sens 7: 169–194
Wiscombe WJ, Warren SG (1980) A model for the spectral albedo of snow. I. Pure snow. J Atmos Sci 37:2712–2733
Yu X, Hyyppä J, Vastaranta M, Holopainen M, Viitala R (2011) Predicting individual tree attributes from airborne laser point clouds based on the random forests technique. ISPRS J Photogramm Remote Sens 66:28–37
Zaitchik BF, Rodell M (2009) Forward-looking assimilation of MODIS-derived snow-covered area into a land surface model. J Hydrometeorol 10:130–148
Zhang G, Xie H, Yao T, Liang T, Kang S (2012) Snow cover dynamics of four lake basins over Tibetan Plateau using time series MODIS data (2001–2010). Water Resour Res 48:W10529

Editorial responsibility: Oliver Frauenfeld, College Station, Texas, USA

Submitted: September 14, 2017; Accepted: May 7, 2018
Proofs received from author(s): July 17, 2018